

Article

Root Canal Obturation by Electrochemical Precipitation of Calcium Phosphates

Maximilian Koch ^{1,†}, Victor Palarie ^{2,†}, Maximilian Göltz ³, Marvin Kurzer ³, Manuel Zulla ³, Stefan Rosiwal ³, Marian Willner ⁴, Andreas Burkovski ⁵ and Matthias Karl ^{6,*}

- ¹ Division of Microbiology, Department of Biology, Friedrich-Alexander-Universität Erlangen-Nürnberg, 91058 Erlangen, Germany; max.koch@fau.de
- ² Laboratory of Tissue Engineering and Cellular Cultures, State University of Medicine and Pharmacy “N. Testemitanu”, 2004 Chisinau, Moldova; vpalarie@gmail.com
- ³ Division of Materials Science and Engineering for Metals, Department of Material Sciences, Friedrich-Alexander-Universität Erlangen-Nürnberg, 91058 Erlangen, Germany; maximilian.goeltz@fau.de (M.G.); marvin.kurzer@fau.de (M.K.); manuel.zulla@fau.de (M.Z.); stefan.rosiwal@fau.de (S.R.)
- ⁴ MITOS GmbH, 85748 Garching b. München, Germany; marian.willner@mitos.de
- ⁵ Professur für Mikrobiologie, Department of Biology, Friedrich-Alexander-Universität Erlangen-Nürnberg, 91058 Erlangen, Germany; andreas.burkovski@fau.de
- ⁶ Department of Prosthodontics, Saarland University, 66421 Homburg/Saar, Germany
- * Correspondence: matthias.karl@uks.eu; Tel.: +49-684-1162-4900
- † These authors contributed equally to the manuscript.

Featured Application: Use of boron-doped diamond electrodes for root canal obturation.

Abstract: Achieving adequate disinfection and preventing reinfection is the major goal in endodontic treatment. Variation in canal morphology and open porosity of dentine prevents achieving complete disinfection. Questionable biocompatibility of materials as well as a lack of sealing ability questions the usefulness of current obturation methods. With a novel disinfection approach based on the use of boron-doped diamond (BDD) electrodes having shown promising results it was the goal of this series of experiments to investigate the possibility of BDD-mediated in situ forming of a biocompatible obturation material. A combination of calcium phosphate and maleic acid was used as precursor solution while Ion Chromatography Mass Spectrometry (IC-MS), Raman spectroscopy (RAMAN), X-ray diffraction (XRD), energy dispersive X-ray spectroscopy (EDX), scanning electron microscopy (SEM), dye penetration and micro-computed tomography (μ CT) were applied for characterizing the precipitate. It was possible to achieve a BDD-mediated precipitation of brushite in a clinically applicable timeframe. However, tight sealing of the canal system based on brushite could not be achieved.

Keywords: boron-doped diamond; brushite; hydroxyapatite; obturation; reactive oxygen species



Citation: Koch, M.; Palarie, V.; Göltz, M.; Kurzer, M.; Zulla, M.; Rosiwal, S.; Willner, M.; Burkovski, A.; Karl, M. Root Canal Obturation by Electrochemical Precipitation of Calcium Phosphates. *Appl. Sci.* **2022**, *12*, 2956. <https://doi.org/10.3390/app12062956>

Academic Editor: Mary Anne Melo

Received: 17 February 2022

Accepted: 9 March 2022

Published: 14 March 2022

Publisher's Note: MDPI stays neutral with regard to jurisdictional claims in published maps and institutional affiliations.



Copyright: © 2022 by the authors. Licensee MDPI, Basel, Switzerland. This article is an open access article distributed under the terms and conditions of the Creative Commons Attribution (CC BY) license (<https://creativecommons.org/licenses/by/4.0/>).

1. Introduction

Current concepts of root canal treatment involve the basic steps of mechanical instrumentation/shaping, cleaning/disinfection and obturation of the canal space. Reinfection of the canal system has to be prevented by sealing the occlusal access. Despite a variety of methods available such as activated rinsing, disinfection of dentin with non-accessible canals and porosities limits the success of endodontic therapy [1–6]. Several authors have pointed out that persisting bacteria may regrow and cause periapical inflammation even if proper obturation has been achieved [7–10]. In this context, the necessity of root canal obturation in general has been questioned [11]. Current experimental approaches are only focusing on the improvement of either disinfection, debridement or obturation [12,13] but do not present a complete treatment solution.

As a novel experimental approach to root canal disinfection, boron-doped diamond (BDD) electrodes have recently been introduced [14]. The major advantage of this method consists in the controlled generation of highly reactive oxygen species directly in the canal system. In order to overcome the two major issues with conventional sealing materials i.e., biocompatibility [15,16] and a lack of sealing ability in non-uniformly shaped root canals [17,18], it was the goal of this experiment to investigate the possibility of in situ forming of a biocompatible obturation. The basic requirements for a BDD-based obturation protocol were identified as follows (i) high precipitation rate of biomaterial, (ii) biocompatibility of the product, (iii) absence of toxic byproducts and (iv) tight and complete seal of the root canal.

Calcium phosphates such as hydroxyapatite constituting the main inorganic component of enamel and bone [19] were identified as ideal candidates to meet these requirements. This group of substances is well known for biocompatibility and has been investigated for a variety of medical applications [20] including toothpastes for triggering remineralization, bone substitutes and coatings of dental implants for optimizing osseointegration [21–24]. In this context, calcium phosphate nanoparticles have been shown to be osteoconductive [25]. Especially brushite, $\text{CaHPO}_4 \times 2 \text{H}_2\text{O}$, can act as a connecting layer binding to enamel, mediating remineralization and undergoing transformation to hydroxyapatite [26–28].

Low solubility of calcium phosphates was identified as the major issue for establishing an in situ formed obturation material. To obtain a higher saturated solution of calcium phosphate, maleic acid was added to act as chelating agent and thereby retarding the precipitation [29,30]. Maleic acid can easily be oxidized by BDD electrodes [31–35], which then triggers the obturation process. With maleic acid being able to dissolve calcium ions from tooth substance and constituting an important component of self-etching dental adhesives [36], sealing of the root canal surface may also benefit from this approach.

This study consisted of several experiments aimed at evaluating the feasibility of BDD-mediated root canal obturation using a calcium phosphate/maleic acid solution. Following formation of the obturation precursor solution, degradation of maleic acid was monitored using Ion Chromatography Mass Spectrometry (IC-MS). The precipitation product was characterized using Raman spectroscopy (RAMAN), X-ray diffraction (XRD) and energy dispersive X-ray spectroscopy (EDX). Reaction tubes and endodontic training blocks were then used for simulating clinical handling conditions, analyzing bonding of the biomaterial to the root canal wall as well as the particle size of the precipitates via scanning electron microscopy (SEM). Sealing capabilities were assessed using dye penetration tests and micro computed tomography (μCT).

2. Materials and Methods

2.1. Chemicals

All chemicals were purchased from Carl Roth GmbH & Co. KG (Karlsruhe, Germany), Merck KGaA (Darmstadt, Germany) and Sigma-Aldrich Chemicals (Munich, Germany).

For preparation of a Ca–maleate precursor solution, calcium carbonate (CaCO_3 , final concentration 0.445 M) was mixed in a molar ratio of 1:2 with maleic acid ($\text{C}_4\text{H}_4\text{O}_4$, final concentration 0.89 M) in deionized water. The mixture was stirred until all components were completely dissolved and CO_2 generation stopped. The Ca–maleate solution was mixed with ammonium dihydrogen phosphate ($\text{NH}_4\text{H}_2\text{PO}_4$, 0.445 M) and diammonium hydrogen phosphate ($(\text{NH}_4)_2\text{HPO}_4$, 0.445 M) in a ratio of 10:8:2 in a reaction tube to give a Ca–phosphate precursor solution with a final Ca/P ratio of 1:1. Ammonium phosphates were mixed (pH 6.5) prior to addition of the Ca–maleate mixture.

2.2. Precipitation Experiments

The precipitation experiments were performed using wound wire BDD electrodes [14,37,38] or glued wire BDD electrodes designed in this study (Figure 1). The BDD-coated niobium wires (200 μm diameter, 2.5 cm length) were produced as previously described [14] and glued together

using cyanoacrylate glue (Sofortkleber, Bindulin-Werk H.L. Schönleber GmbH, Fürth, Germany) for a narrow cross section of approximately 500 μm).

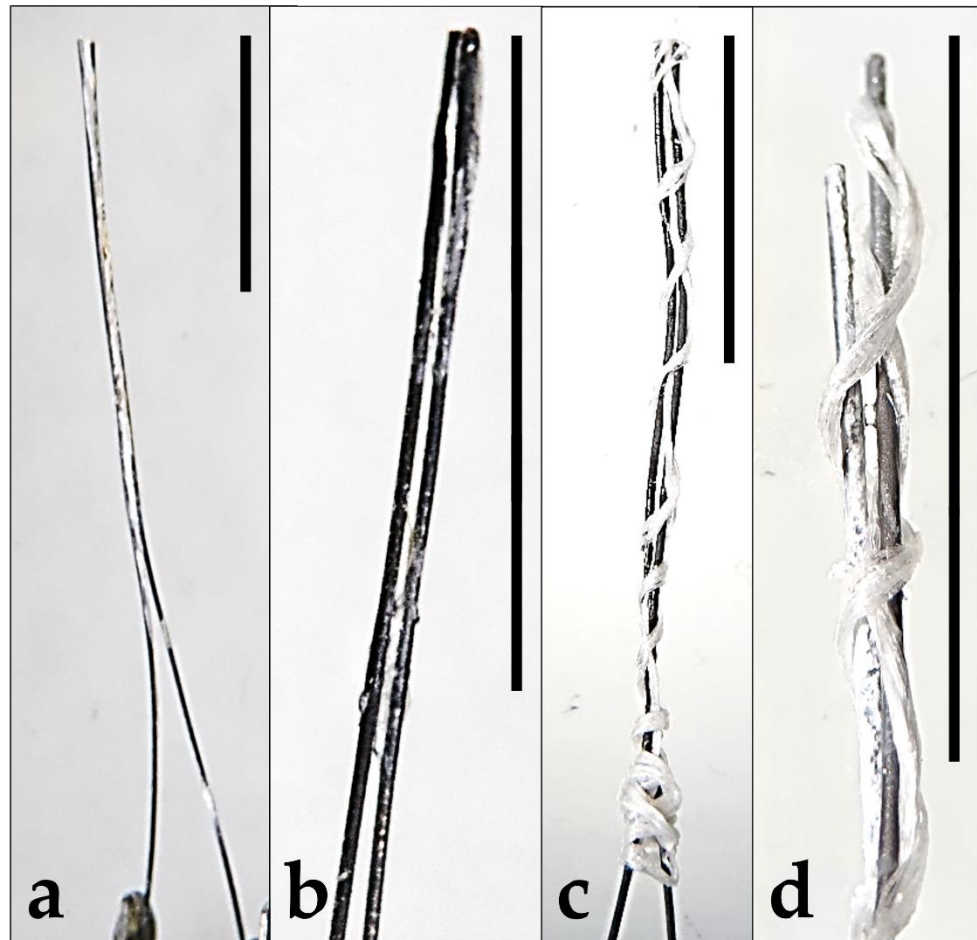


Figure 1. BDD electrodes used for initiation of precipitation. (a,b) Glued wire electrode (this work); (c,d) wound wire electrode. Scale bars represent 1 cm.

For precipitation in reaction tubes, electrodes (Figure 1) were immersed in CaP precursor solution (2 mL). A constant potential was applied to the electrodes (6–16 V, 2 min) using a laboratory power supply (H/H switch power supply PS2002H, Komerici GmbH & Co.KG, Ebern, Germany). Initiation of precipitation was independent of the used electrode type (glued or wound) but strictly dependent on the applied current. After centrifugation ($10,000\times g$, 10 s) the supernatant was removed and stored for IC-MS measurements. The precipitate was washed three times with deionized water, dried under vacuum in a desiccator ($65\text{ }^{\circ}\text{C}$) and stored (RT, desiccator) for further analysis with SEM, EDX, XRD and RAMAN.

To test the applicability of BDD-mediated precipitation in a restricted volume, endodontic training blocks (HyFlex CM Endo Practice Block, Coltene Whaledent, Altstätten, Switzerland) were prepared using standard reciprocating files (Reciproc R50, VDW, Munich, Germany). The apical opening of the simulated root canal was transitionally sealed using commercially available plasticine. CaP precursor solution was added using a syringe and the glued-wire BDD electrode was inserted into the solution. A constant potential (9, 11 and 15 V) was applied to the electrode. During precipitation, the precursor solution was constantly added, and the precipitate was condensed using a plugger (Figure 2). After the apical third was sealed, excess liquid was removed using paper points (Reciproc R 25, VDW GmbH, Munich, Germany).

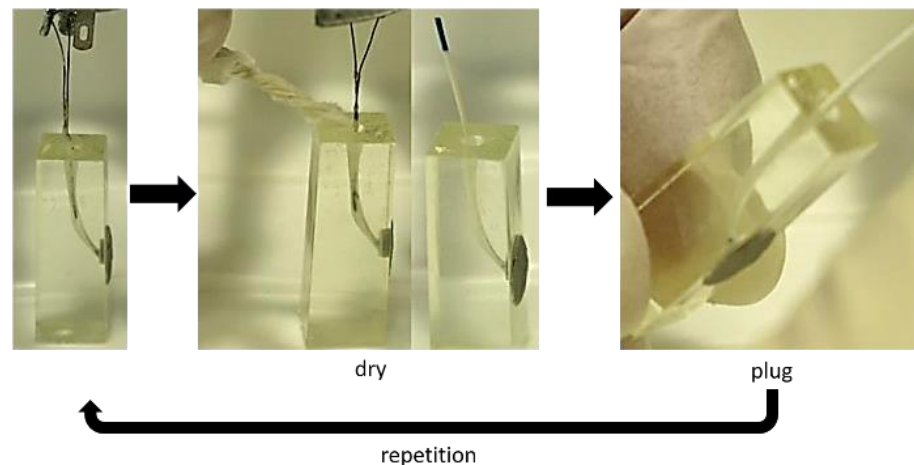


Figure 2. Obturation procedure for the endo practice blocks. The canals were filled with CaP precursor solution and the glued wire BDD prototype was inserted into the canal. The precipitate was dried and condensed before starting the next precipitation cycle until the apical third was filled with precipitate.

As last approach, the roots from three carious-free extracted human teeth were obtained by horizontal cutting at the cementum-enamel junction using a diamond band saw (EXAKT 300, EXAKT Advanced Technologies, Norderstedt, Germany). Root canals were subsequently prepared using reciprocating files (Reciproc R50, VDW, Munich, Germany) and conventional rinsing (sodium hypochlorite, chlorhexidine, ethanol). The prepared teeth were autoclaved (20 min, 121 °C) in distilled water and stored at ambient temperature until use. The roots were then positioned in modeling clay (Figure 3), CaP precursor solution (20 μ L) was added using a syringe and the glued-wire BDD electrode was inserted into the canal. A constant potential (12 V) was applied to the electrode. The precursor solution was constantly added (20 μ L, multiple times) to the root canal, after drying and plugging the precipitate from the prior precipitation phase until the root canal was filled completely. The filled roots were dried and stored at ambient temperature until μ CT analysis.



Figure 3. Obturation procedure for extracted human teeth. The roots were placed in modeling clay, the CaP precursor was added into the canal using a syringe and the BDD-electrode was applied. Scale bar: 1 cm.

2.3. Analysis of Precipitation Products

2.3.1. RAMAN Spectroscopy

Spectra were recorded on a confocal Raman microscope (LabRAM ARAMIS, Horiba Jobin–Yvon, Villeneuve d’Ascq, France). A diode-pumped solid-state (DPSS) laser (mpc

6000, Laser Quantum Ltd., Stockport, England) generated the excitation wavelength of 532 nm. A 10× objective (MPlan N 10×, 0.25 NA, Olympus Deutschland GmbH, Hamburg, Germany) was used. Two spectra were recorded from one acquisition (10 s, RT), the confocal hole (300 μm) and the entrance slit (100 μm) of the monochromator were fixed [39].

2.3.2. SEM/EDX Spectroscopy

Dried samples were analyzed by scanning electron microscopy (SEM, FEI Quanta 450, FEI Deutschland GmbH, Frankfurt, Germany). Images were taken by applying the Everhart-Thornley detector (ETD) back-scatter detector (BSE) combination [40]. The precipitate samples and all comparison samples were screened extensively and elemental analysis was performed with energy-dispersive X-ray spectroscopy (EDX) [41].

2.4. Analysis of Maleate Degradation

Maleate degradation in supernatants was monitored applying ion chromatography with an ICS 3000 (Dionex, Thermo Fischer Scientific, Wesel, Germany) and ESI/MS/MS detection using a QTrap3200 Triple-Quadrupole mass spectrometer with turbo V ion source (Applied Biosystems, Thermo Fischer Scientific, Wesel, Germany) operated in multiple reaction monitoring mode.

2.5. Characterization of Sealing Quality

2.5.1. Dye Penetration Test

Dye penetration tests were performed by submerging previously filled endo practice blocks in MIRA-2-TON plaque disclosing solution (Hager & Werken GmbH & Co. KG, Duisburg, Germany) for 24 h. The outcome was assessed via penetration depth measurements and imaged using a stereomicroscope (Nikon SMZ-745T, Nikon Metrology GmbH, Düsseldorf, Germany).

2.5.2. Imaging Analysis of Precipitate Density

SEM imaging was performed as described above. X-ray imaging was performed using a conventional dental X-ray unit (Heliodent Plus, Dentsply Sirona, Bensheim) and intraoral image plates (VistaScan, Dürr Dental, Bietigheim-Bissingen). Micro-CT measurement for sealing quality was performed using a Siemens Inveon PET/SPECT/CT (Siemens Healthcare GmbH, Erlangen, Germany). The X-ray tube voltage and current were set to 80.0 kV and 500 μA, respectively. The resolution was 13.1 μm at a total scan duration of 39.0 min. The Inveon Acquisition Workplace software was used for process controlling and monitoring. The image analysis was performed using the RadiAnt DICOM Viewer (Medixant, Poznan, Poland) to reconstruct 3D data [7,42,43].

For X-ray micro-tomography characterization of material distribution within the root canal, i.e., porosity of filling, μCT scans were performed on a ZEISS Xradia 500 Versa equipped with a 160 kV transmission tube and an indirect detection system made of a scintillator, switchable objective lenses (0.39×, 4×, 20×) and a CCD camera with 2048 × 2048 pixels. Each tooth was attached to the sample holder with the crown down with no specific preparation being needed. The samples were imaged at a source-to-sample distance of 17 mm and a sample-to-detector distance of 12 mm. The 4× objective and a 2-fold detector binning (1024 × 1024) were used for the acquisition, resulting in an effective pixel size of 4 μm. The tomographic scans included 1801 radiographic projection images that were recorded over a sample rotation of 360° and with an exposure time of 2 s per image. The tube voltage and power were 80 kV and 6 W, respectively. Tomographic reconstruction of the acquired data and further data processing was carried out with the software X-AID (MITOS GmbH, Garching, Germany). The filtered back-projection algorithm for local tomographies was applied in combination with the beam hardening correction for cupping artefacts. The initial datasets were cropped to 850 × 500 × 500 voxels during reconstruction. Thus, the final volumes consist of 850 stacked images of dimensions 2 × 2 mm and cover a total height of 3.4 mm. The gray values of the reconstructed images

relate to differences in X-ray attenuation of the respective materials and certain features like the pores within the filling can be segmented based on grayscale thresholds. In the first step, image noise was reduced by using a bilateral post-processing filter to enable better segmentation. Binary volumes masking the root canals were created the following: (i) Segmenting the tooth material by manual thresholding. (ii) Removing segmented structures of similar grey values within the root canals by applying morphological operations like the opening operation. (iii) Inverting the resulting images. (iv) Removing remaining regions outside of the root canals. Binary volumes representing the pores were obtained by Otsu thresholding on the grey value distributions within the root canals. The volume fractions of the pores within the root canals were determined by relating the voxels belonging to the pores in the root canals to the total number of voxels in the root canals. For the analysis, the sample volumes were divided into blocks of 50 images, corresponding to section of 200 μm . Omitting the first and last sections, 15 values were evaluated over a range of 3 mm for each sample.

3. Results

3.1. Maleic Acid as BDD Electrode-Degradable Retardant

Due to its low solubility calcium phosphate tends to precipitate even in low concentrated solution. Stabilization of such solutions can be reached using Ca^{2+} chelators. A precursor solution based on maleic acid was stable over a period of one hour, while precipitation from an originally supersaturated solution was achieved by BDD electrode treatment (Figure 4).

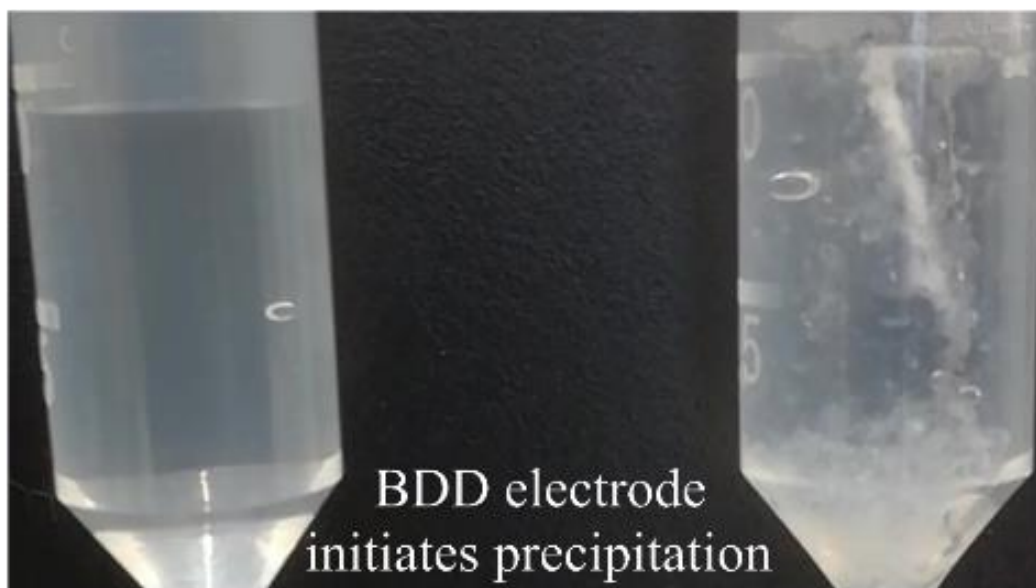


Figure 4. Comparison of CaP precursor solution before (left) and during (right) BDD electrode application. The left CaP precursor was stable through the whole time of the experiment, while precipitation of CaP started directly after current application.

To validate that degradation of the stabilizer maleic acid is responsible for calcium phosphate precipitation, further experiments were carried out. A quantitative analysis of the maleate concentration in the supernatants after application of different potentials showed a clear BDD electrode-dependent degradation of maleic acid (Figure 5). As shown above, calcium phosphates were precipitated with onset of BDD electrode treatment (Figure 5). As in the case of maleic acid concentration, a direct correlation of BDD electrode treatment and precipitation of calcium phosphates was found (Figure 5).

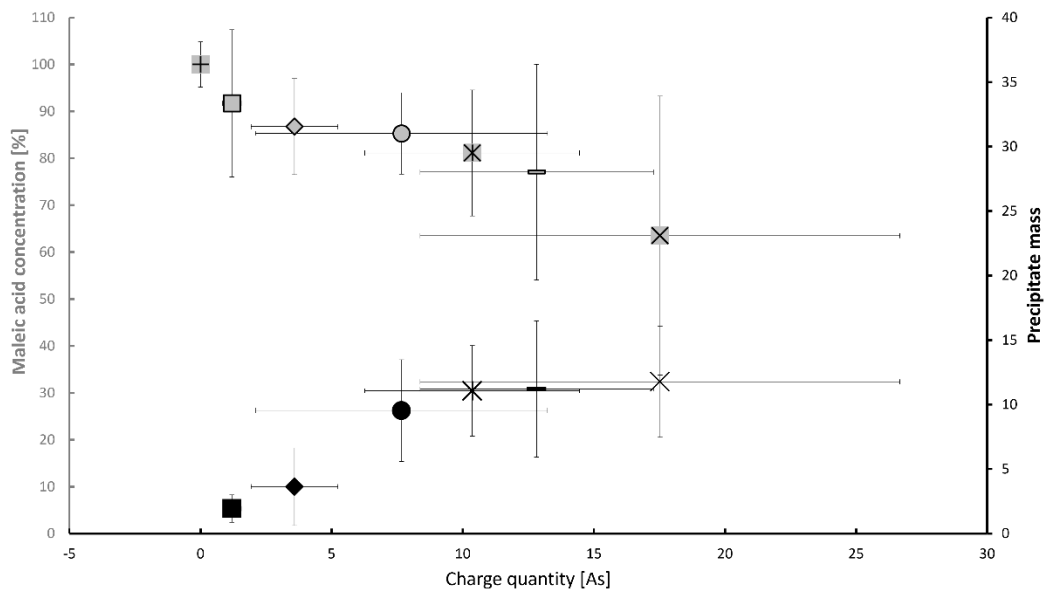


Figure 5. Relative maleic acid degradation and precipitate mass production in relation to the applied charge quantity. Black data points: Precipitate mass after two minutes of BDD application to two milliliters of the CaP precursor solution. Different potentials (rsp. currents) were applied to the electrode. Interestingly there is a purported decrease of precipitation efficiency at charge quantities higher than 15 As. This may indicate a lower efficiency of the electrode itself due to surface reduction, as the precipitate is blocking cathode space. Another possible explanation could be an increase in oxygen production leading to a lower degradation of maleate via reactive oxygen species. Mean concentration of maleic acid (grey symbols) and CaP mass (black symbols) depending on mean charge quantities applied is shown; the data indicate that the amount of maleate degradation is directly correlated with the precipitate formation of calcium phosphate.

3.2. Analysis of Precipitated Calcium Phosphate Salts

Calcium phosphate salts may differ significantly in their specific composition. The precipitates were therefore further analyzed. As a first approach, precipitates were analyzed via SEM and energy dispersive X-ray spectroscopy (EDX) (Figure 6). Flower-like crystal structures and the observed average Ca/P ratio of 1 may hint to brushite [40,41]. However, statistical analyses ($n = 18$) of the results obtained revealed a standard deviation of 0.02, leaving room for the presence of other calcium phosphate salts.

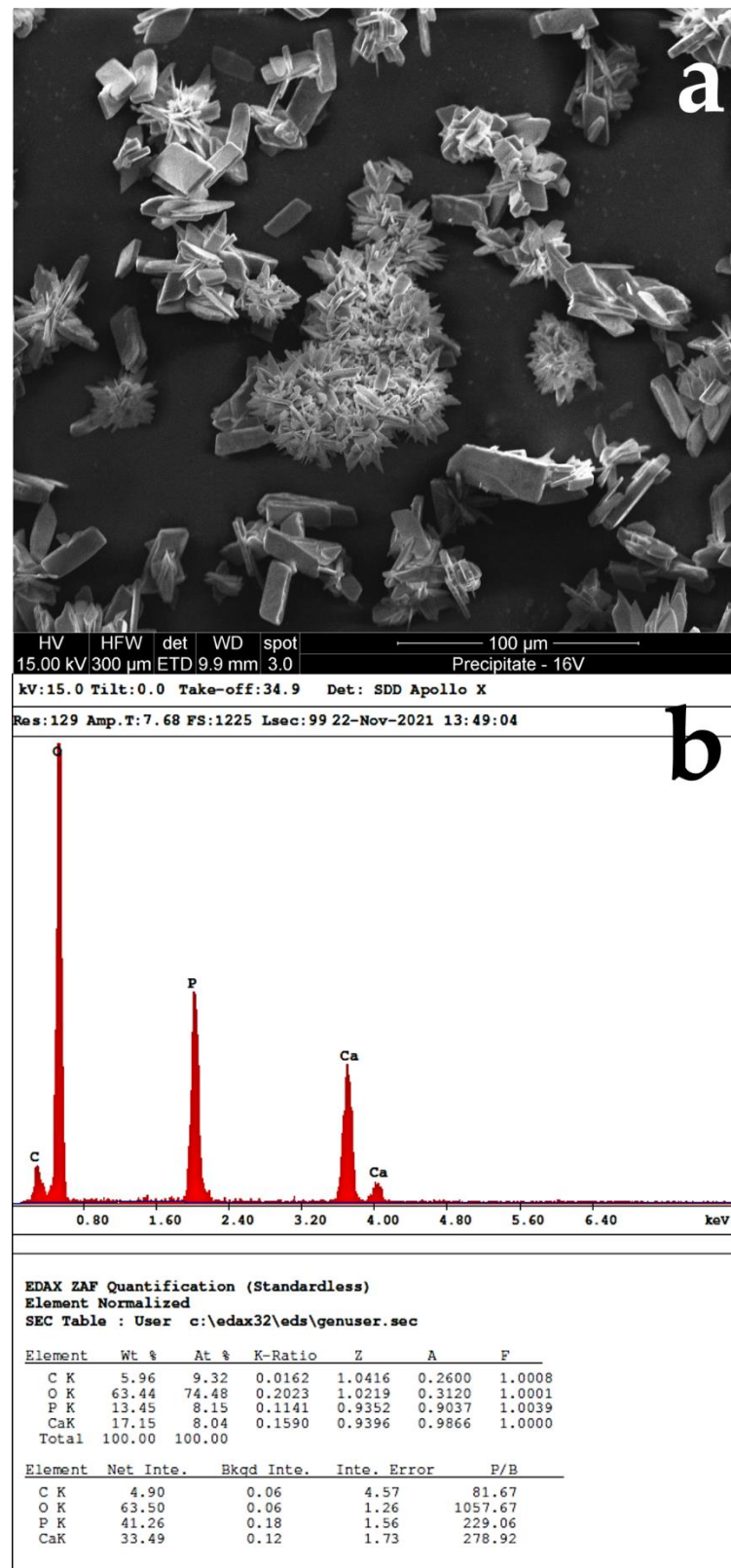


Figure 6. CaP precipitate analysis via SEM and energy dispersive X-ray spectroscopy (EDX). (a) Typical plate and flower like structures are observed in the SEM image. (b) The respective EDX scan shows a Ca/P ratio of 1.11.

SEM/EDX analyses indicated brushite as precipitated material. To unequivocally identify the precipitated calcium phosphate species, XRD analyses were carried out. Both,

data base spectra and spectra of commercially available brushite corresponded exactly to the precipitated material (Figure 7).

Calcium Phosphate Precipitate vs. Brushit

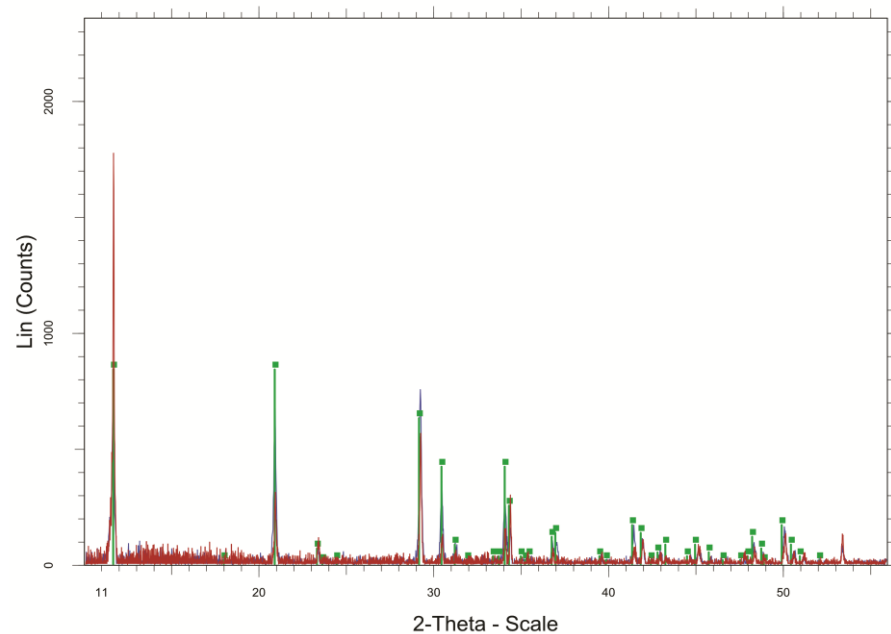


Figure 7. CaP precipitate phase identification as brushite via X-ray powder diffraction (XRD) [40]. Background and $K\alpha$ -stripping were corrected. Red: CaP precipitate sample. Blue: comparison measurement of brushite (Carl Roth GmbH & Co. KG, Karlsruhe, Germany). Green: Brushite reference spectrum from the database of the International Center for Diffraction Data (ICDD).

In a last step, RAMAN spectroscopy was applied for a fast and reliable comparison of precipitates obtained after BDD-induced precipitation [44–47]. Electrical potentials between 6 and 16 V applied during the precipitation. Again, data base spectra and spectra of commercially available brushite corresponded exactly to the precipitated material independent of the applied charge (Figure 8).

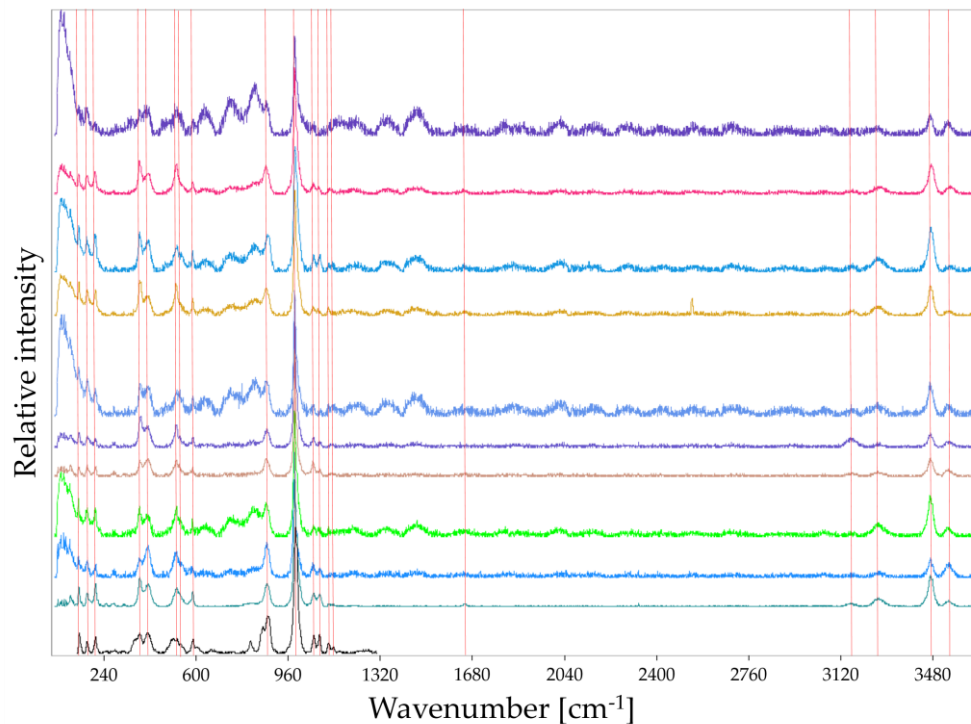


Figure 8. Precipitate analysis via RAMAN spectroscopy. All sample data were background corrected using Crystal Sleuth software provided by the RRUFF Project [45]. Raman scans of brushite taken from the RRUFF Database (black line, RRUFF ID: R070554), positive sample (petrol, Carl Roth GmbH & Co. KG, Karlsruhe, Germany), precipitates at 6 V (blue), 8 V (green), 9 V (brown), 10 V (purple), 11 V (deep blue), 12 V (orange), 14 V (pale blue), 15 V (red) and 16 V (deep purple). Vertical red lines show matching peaks with database sample and positive sample. Experiments were carried out in triplicate and typical spectra are shown.

3.3. Obturation of Root Canals

The volume available in the root canal cannot bear such an amount of precursor solution which is sufficient for root canal obturation. This resulted in the need for repeatedly applying precursor solution following precipitation and removal of fluids. Brushite initially precipitate at the surface of the BDD electrodes (Figure 9) but continuing treatment leads to deposition of biomaterial in the canal lumen (Figure 10). Characterization of these brushite depots by SEM revealed a close connection to the wall of the root canal and sealing of dentin tubules (Figure 11).

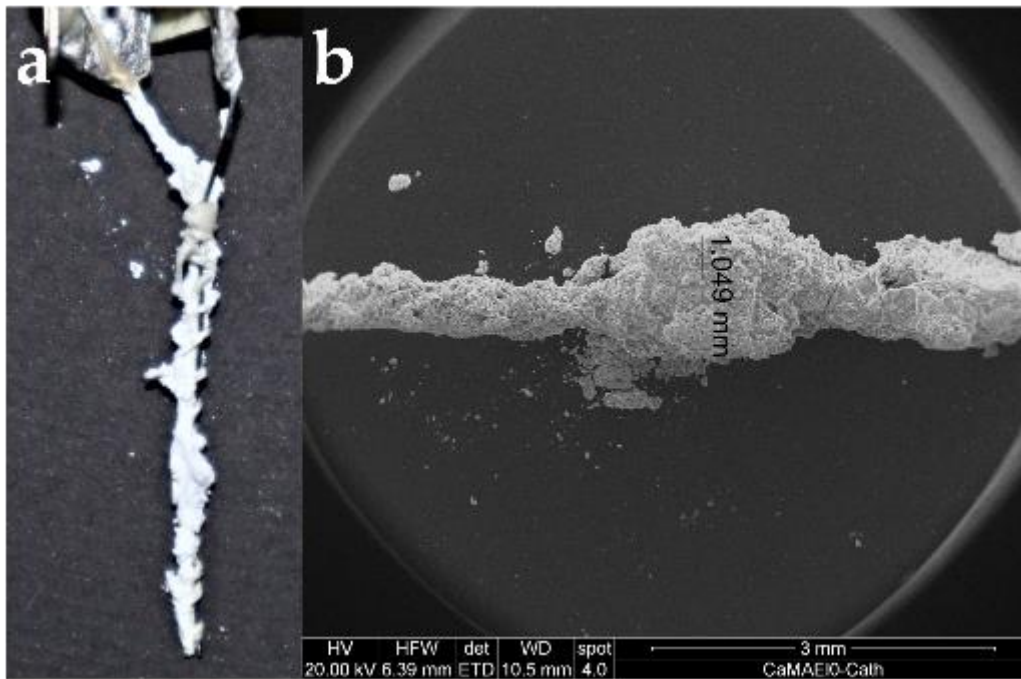


Figure 9. Precipitation of brushite by a BDD electrode. Initial deposition of CaP at the cathode surface. (a) Cathode of the “wound-wire electrode” covered in precipitate. Please note that the anode is free of precipitate. (b) SEM micrograph of precipitate formed after a few seconds of current applied. Parameters are shown in the box at the bottom. ETD: Everhart-Thornley detector.

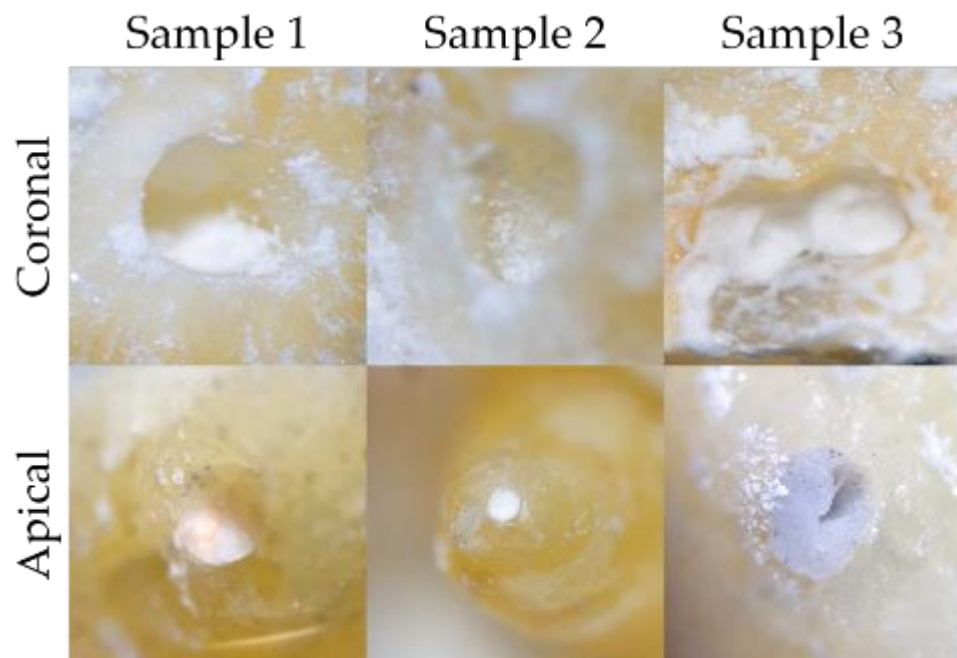


Figure 10. Apical and coronal microscopic views of root canals from extracted human teeth following BDD-mediated obturation.

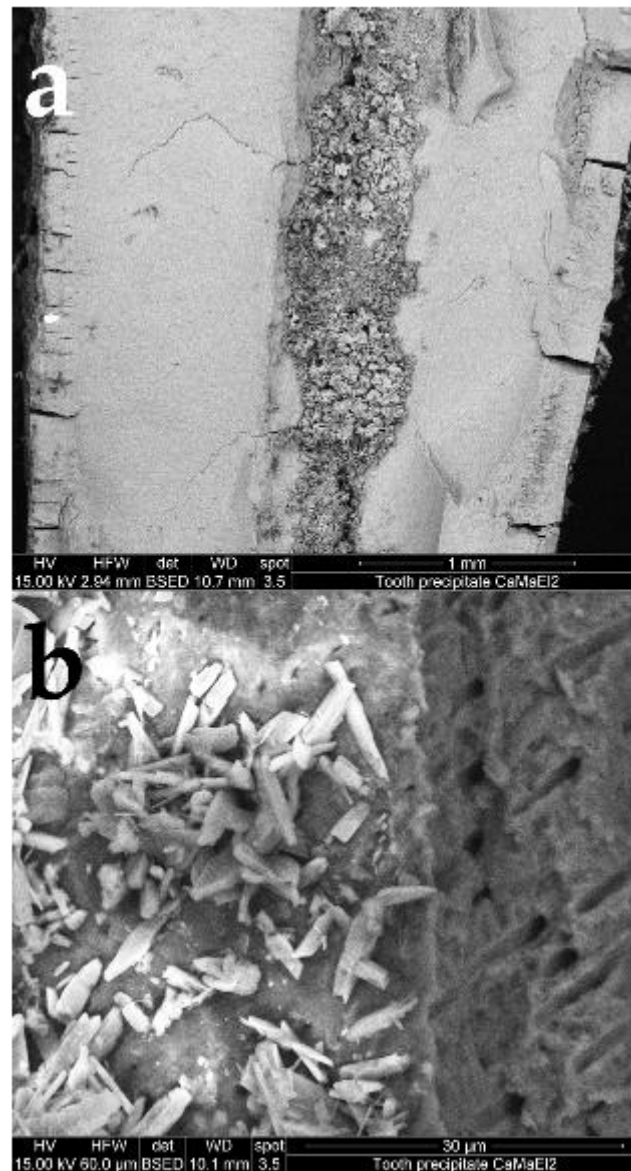


Figure 11. SEM image of tooth split in half after CaP obturation. The tooth was dried at 65 °C for 48 h prior to SEM imaging. Loose crystals were removed using compressed air. (a) Filled root canal; (b) crystals attaching to the root canals sealing the dentin tubules (left: crystals at the root canal surface; right: cross section of the dentin tubules). BSED: back-scatter detector.

With brushite being an electron-dense material, obturation of root canals can be verified radiographically. When sealing quality was monitored by X-ray and μ CT scans, for endodontic training blocks and extracted human teeth, BDD-mediated root canal obturation was visible in conventional with both methods (Figures 12 and 13). In addition, μ CT scans revealed maximal distance below 100 μ m between precipitate and canal wall (Figure 12).

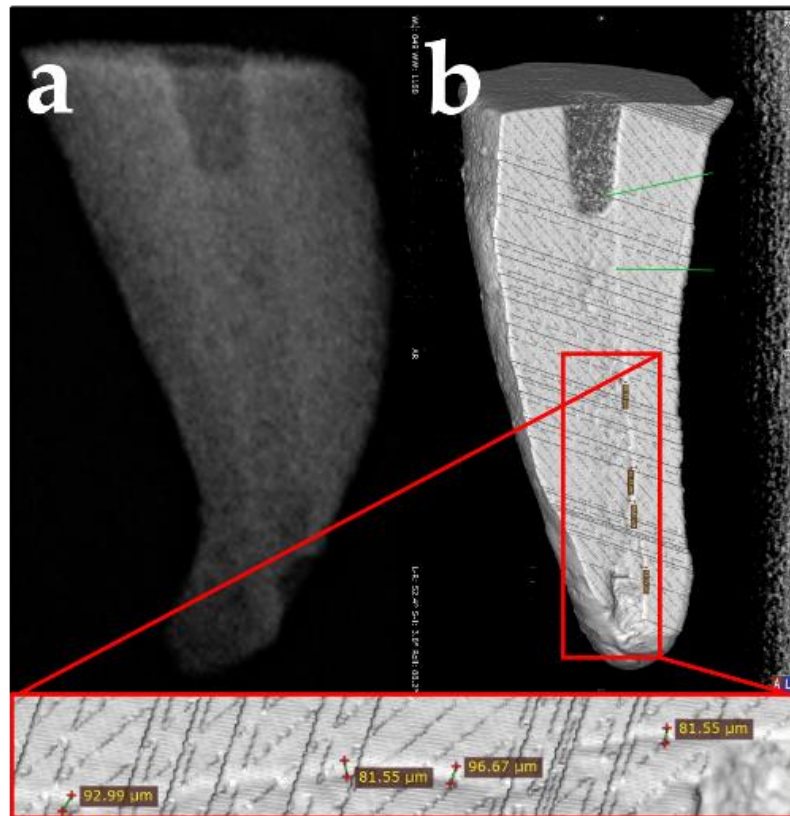


Figure 12. Determination of the sealing quality in root canals. (a) X-ray images; (b) μ CT images of obturated root canals.

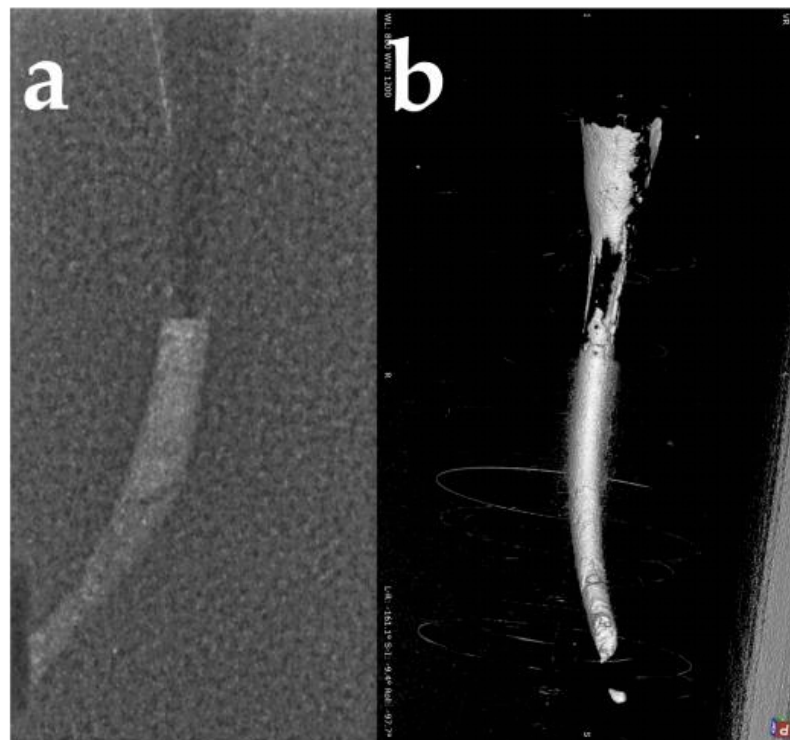


Figure 13. Determination of the sealing quality in endo training blocks. (a) X-ray images; (b) μ CT images of obturated endo training blocks.

For analysis of porosity, tomographic reconstruction of acquired μ CT data and further data processing was carried out with the software X-AID (Figure 14). A total of 15 values were evaluated over a range of 3 mm for each sample ($n = 3$). For the precipitated material, an overall porosity of 11.27% with a standard deviation of $\pm 7.47\%$ was obtained.

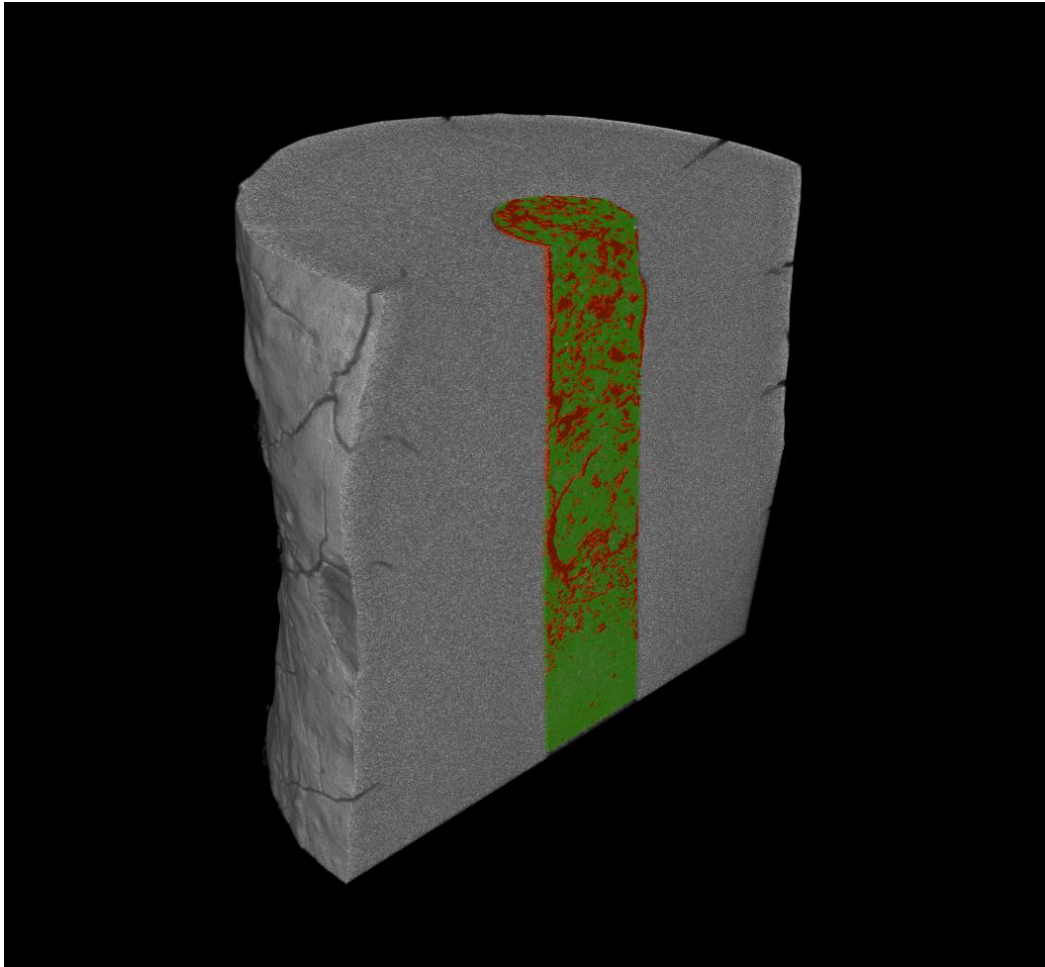


Figure 14. Porosity analysis of BDD-dependent brushite precipitation. Tomographic reconstruction of μ CT data and further data processing was carried out using the X-AID software (MITOS GmbH, Garching, Germany). Pores are indicated in red, solid material in green.

3.4. Dye Penetration Test

Dye penetration tests revealed apical leakage of the obturation material as may have been expected due to the hydrophilic nature of Ca-phosphate (Figure 15)

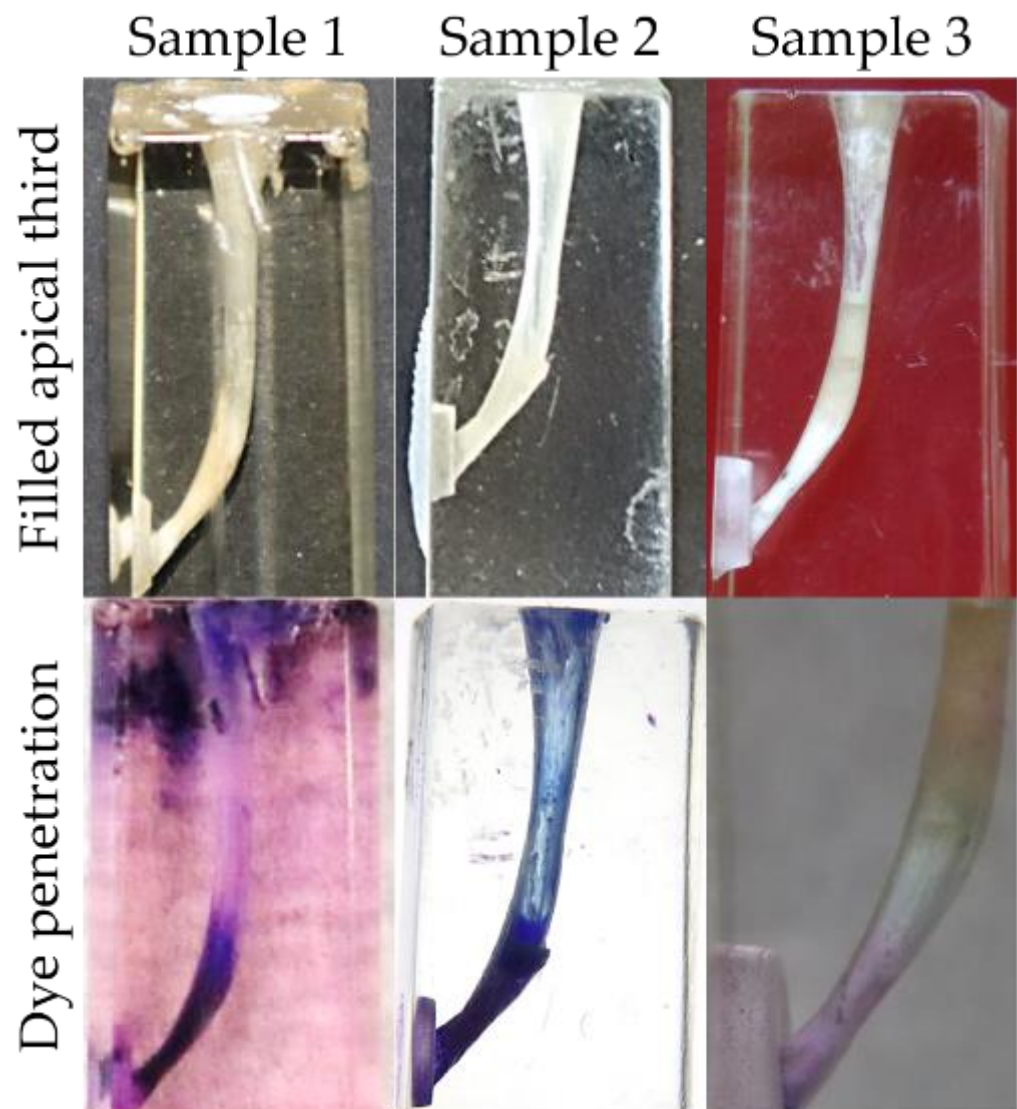


Figure 15. Results of dye penetration tests in endo training blocks following BDD-mediated root canal obturation. As expected, complete penetration was visible in all instances.

4. Discussion

Using maleic acid [36] as chelating agent, it was possible to establish a chemically stable but highly saturated calcium phosphate solution. Application of a BDD electrode led to the oxidation of maleic acid and precipitation of biocompatible brushite on the electrode surface and inside the root canal. A binding to the root canal wall, as seen in Figure 11, may be the effect of maleic acid as self-etching primer [36].

The reaction for the assumed complex formation which is responsible for the retardation effect is shown in Figure 16. The application of a BDD electrode leads to oxidation of the chelating agent and a following complete decomposition to CO_2 [31–34], releasing the calcium ion from the complex. The free calcium ion then forms solid brushite with the hydrogen phosphate anion as soon as the solubility product is reached. An evolution of a significant amount of toxic byproducts is not expected due to a complete degradation of the maleate to CO_2 [31,33,34,36].

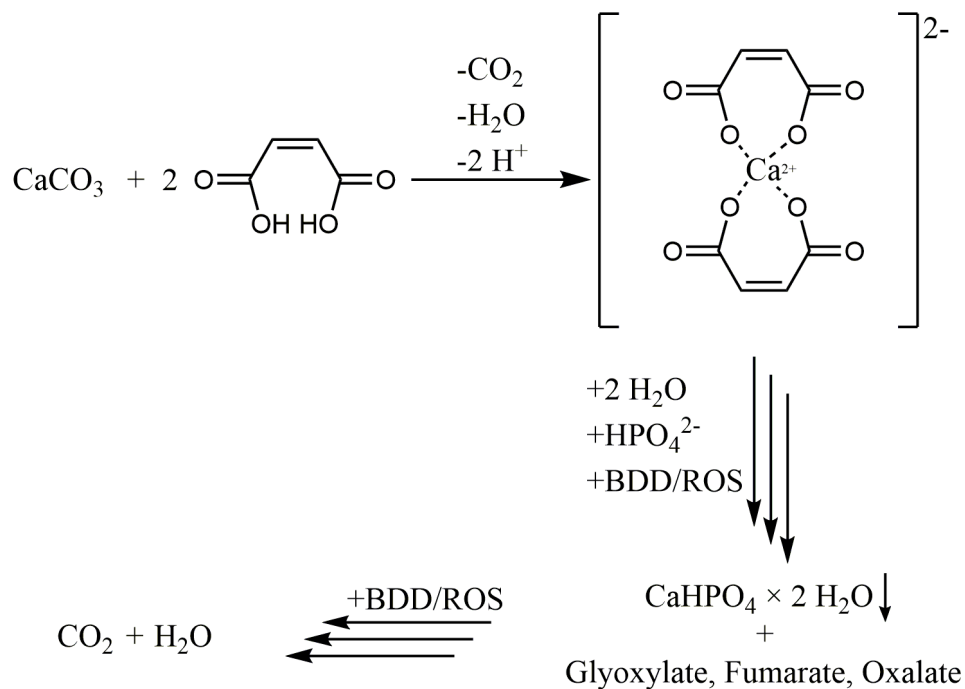


Figure 16. Proposed reaction pathway of complex building and BDD mediated decomposition. The formation of a calcium maleate complex prevents the precipitation in the highly supersaturated solution (referred to as brushite and other calcium phosphates).

The amount of formed precipitate can be controlled by the applied current and application time, and the precipitation currently has a purported efficiency maximum at around 30% (Figure 5). Also, the applicability of higher potentials and charge quantity is limited due to heat formation during the precipitation process. Therefore, a lower current and longer precipitation period is more useful.

From a handling perspective, the precipitation was achieved within a reasonable timeframe. The root canal obturation required repeated application of precursor solution, BDD application, drying with paper points and plugging.

The obturation material was closely attached to the canal walls and was visible on X-ray images. Due to the hydrophilic nature of Ca phosphate, complete penetration of the filling was possible. It may be argued whether this is problematic [11]. Assuming complete disinfection of root canals prior to obturation, bacteria should have also been eliminated from the periapical region. Penetration of body fluids into the obturation material may be not problematic as brushite is biocompatible in contrast to current sealing materials [15,16].

5. Conclusions

In addition to the previously discussed applications in endodontic and peri-implantitis treatment, BDD electrodes have shown promising results in this study investigating the possibility of BDD-mediated in situ formation of bio-compatible obturation material. A combination of calcium phosphate and maleic acid was used as precursor solution and BDD-mediated precipitation of brushite was observed within a few minutes. The results obtained may provide an excellent basis for the development of a clinically applicable protocol.

Author Contributions: Conceptualization, M.K. (Maximilian Koch); A.B. and M.K. (Matthias Karl); methodology dental, V.P. and M.K. (Maximilian Koch); methodology chemical and biological, M.K. (Maximilian Koch); methodology material, M.W., M.K. (Maximilian Koch), M.G. and M.K. (Marvin Kurzer); preparation of diamond wires, M.G. and M.Z.; investigation, V.P. and M.K. (Maximilian Koch); resources, A.B. and S.R.; data curation, V.P. and M.K. (Maximilian Koch); writing—original draft preparation, A.B., M.K. (Matthias Karl) and M.K. (Maximilian Koch); writing—review and editing, A.B. and M.K. (Matthias Karl); supervision, A.B., M.K. (Matthias Karl) and S.R.; funding acquisition, A.B., M.K. (Matthias Karl) and V.P. All authors have read and agreed to the published version of the manuscript.

Funding: The project was funded by Forschungsgemeinschaft Dental e.V. (Grant No. 01/2020) and the Dr. Rolf M. Schwiete Stiftung (Grant 2020-037).

Institutional Review Board Statement: The teeth used in this study were extracted during regular treatments of various patients and stored for research and educational purposes. Ethics committee approval was not required for the study presented.

Informed Consent Statement: Not applicable.

Acknowledgments: We thank David Rüscher (Division of Biochemistry, Friedrich-Alexander-Universität Erlangen-Nürnberg, 91058 Erlangen, Germany), who kindly provided the IC-MS measurements.

Conflicts of Interest: The authors A.B., S.R. and M.K. disclose a conflict of interest as inventors of BDD electrodes for dental applications.

References

- Bergenholtz, G.; Spångberg, L. Controversies in endodontics. *Crit. Rev. Oral Biol. Med.* **2004**, *15*, 99–114. [[CrossRef](#)] [[PubMed](#)]
- Gu, L.-S.; Kim, J.R.; Ling, J.; Choi, K.K.; Pashley, D.H.; Tay, F.R. Review of contemporary irrigant agitation techniques and devices. *J. Endod.* **2009**, *35*, 791–804. [[CrossRef](#)] [[PubMed](#)]
- Löst, C. Quality guidelines for endodontic treatment: Consensus report of the european society of endodontology. *Int. Endod. J.* **2006**, *39*, 921–930.
- Pedrazzi, V.; Oliveira-Neto, J.M.; Sequeira-Byron, P.; Fedorowicz, Z.; Nasser, M. Hand and ultrasonic instrumentation for orthograde root canal treatment of permanent teeth. *Cochrane Database Syst. Rev.* **2019**, *2*, CD006384. [[CrossRef](#)]
- Peters, O.A. Current challenges and concepts in the preparation of root canal systems: A review. *J. Endod.* **2004**, *30*, 559–567. [[CrossRef](#)]
- Siqueira, J.F.; Rôças, I.N.; Ricucci, D. Internal tooth anatomy and root canal instrumentation. In *The Root Canal Anatomy in Permanent Dentition*, 1st ed.; Versiani, M.A., Basrani, B., Sousa-Neto, M.D., Eds.; Springer: Cham, Switzerland, 2018; pp. 277–302.
- Burkovski, A.; Karl, M. Lack of evidence for the necessity of root canal obturation. *Quintessence Int.* **2019**, *50*, 22–28.
- Hamedy, R.; Shakiba, B.; White, S.N. Essential elder endodontics. *Gerodontology* **2016**, *33*, 433. [[CrossRef](#)] [[PubMed](#)]
- Laukkanen, E.; Vehkalahti, M.M.; Kotiranta, A.K. Radiographic outcome of root canal treatment in general dental practice: Tooth type and quality of root filling as prognostic factors. *Acta Odontol. Scand.* **2021**, *79*, 37–42. [[CrossRef](#)]
- Zandi, H.; Petronijevic, N.; Mdala, I.; Kristoffersen, A.K.; Enersen, M.; Rôças, I.N.; Siqueira, J.F.; Ørstavik, D. Outcome of endodontic retreatment using 2 root canal irrigants and influence of infection on healing as determined by a molecular method: A randomized clinical trial. *J. Endod.* **2019**, *45*, 1089–1098.e5. [[CrossRef](#)]
- Sabeti, M.A.; Nekofar, M.; Motahary, P.; Ghandi, M.; Simon, J.H. Healing of apical periodontitis after endodontic treatment with and without obturation in dogs. *J. Endod.* **2006**, *32*, 628–633. [[CrossRef](#)] [[PubMed](#)]
- Keskin, G.; Çiloğlu, M. Efficacy of antimicrobial photodynamic therapy and Er, Cr:YSGG laser-activated irrigation on dentinal tubule penetration of MTA-based root canal sealer: A confocal microscopy study. *Photodiagn. Photodyn. Ther.* **2021**, *36*, 102584. [[CrossRef](#)] [[PubMed](#)]
- Zeng, C.; Everett, J.; Sidow, S.; Bergeron, B.E.; Tian, F.; Ma, J.; Tay, F.R. In vitro evaluation of efficacy of two endodontic sonic-powered irrigant agitation systems in killing single-species intracanal biofilms. *J. Dent.* **2021**, *36*, 103859. [[CrossRef](#)] [[PubMed](#)]
- Böhm, A.L.; Koch, M.; Rosiwal, S.; Burkovski, A.; Karl, M.; Grobecker-Karl, T. Electrochemical disinfection of experimentally infected teeth by boron-doped diamond electrode treatment. *J. Clin. Med.* **2019**, *8*, 2037. [[CrossRef](#)]
- Kolokuris, I.; Beltes, P.; Economides, N.; Vlemmas, I. Experimental study of the biocompatibility of a new glass-Ionomer root canal sealer (Ketac-Endo). *J. Endod.* **1996**, *22*, 395–398. [[CrossRef](#)]
- Scarpato, R.K.; Soares Grecca, F.; Vianna, E.; Fachin, F. Analysis of tissue reactions to methacrylate resin-based, epoxy resin-based, and zinc oxide-eugenol endodontic sealers. *J. Endod.* **2008**, *35*, 229–232. [[CrossRef](#)] [[PubMed](#)]
- Li, G.H.; Niu, L.N.; Zhang, W.; Olsen, M.; De-Deus, G.; Eid, A.A.; Chen, J.H.; Pashley, D.H.; Tay, F.R. Ability of new obturation materials to improve the seal of the root canal system—A review. *Acta Biomater.* **2014**, *10*, 1050. [[CrossRef](#)]

18. Signoretti, F.G.C.; Endo, M.S.; Gomes, B.P.F.A.; Montagner, F.; Tosello, F.B.; Erio, R.; Jacinto, C. Persistent extraradicular infection in root-filled asymptomatic human tooth: Scanning electron microscopic analysis and microbial investigation after apical microsurgery. *J. Endod.* **2011**, *37*, 1696–1700. [[CrossRef](#)]
19. Zhao, J.; Liu, Y.; Sun, W.-B.; Zhang, H. Amorphous calcium phosphate and its application in dentistry. *Chem. Cent. J.* **2011**, *5*, 40. [[CrossRef](#)]
20. Habraken, W.; Habibovic, P.; Epple, M.; Bohner, M. Calcium phosphates in biomedical applications: Materials for the future? *Mater. Today* **2016**, *19*, 69–87. [[CrossRef](#)]
21. Amaechi, B.T.; AbdulAzees, P.A.; Alshareif, D.O.; Shehata, M.A.; Lima, P.P.d.C.S.; Abdollahi, A.; Kalkhorani, P.S.; Evans, V. Comparative Efficacy of a hydroxyapatite and a fluoride toothpaste for prevention and remineralization of dental caries in children. *BDJ Open* **2019**, *5*, 18. [[CrossRef](#)]
22. Jung, S.; Sielker, S.; Hanisch, M.R.; Libricht, V.; Schäfer, E.; Dammaschke, T. Cytotoxic effects of four different root canal sealers on human osteoblasts. *PLoS ONE* **2018**, *13*, e0194467. [[CrossRef](#)] [[PubMed](#)]
23. Pepla, E. Nano-hydroxyapatite and its applications in preventive, restorative and regenerative dentistry: A review of literature. *Ann. Stomatol.* **2014**, *5*, 108–114. [[CrossRef](#)]
24. Pobloth, A.M.; Mersiowsky, M.J.; Kliemt, L.; Schell, H.; Dienelt, A.; Pfitzner, B.M.; Burgkart, R.; Detsch, R.; Wulsten, D.; Boccaccini, A.R.; et al. Bioactive coating of zirconia toughened alumina ceramic implants improves cancellous osseointegration. *Sci. Rep.* **2019**, *9*, 16692. [[CrossRef](#)] [[PubMed](#)]
25. Bayani, M.; Torabi, S.; Shahnaz, A.; Pourali, M. Main properties of nanocrystalline hydroxyapatite as a bone graft material in treatment of periodontal defects. A review of literature. *Biotechnol. Biotechnol. Equip.* **2017**, *31*, 215–220. [[CrossRef](#)]
26. Abbassy, M.A.; Bakry, A.S.; Almoabady, E.H.; Almusally, S.M.; Hassan, A.H. Characterization of a novel enamel sealer for bioactive remineralization of white spot lesions. *J. Dent.* **2021**, *109*, 103663. [[CrossRef](#)] [[PubMed](#)]
27. Bakry, A.S.; Takahashi, H.; Otsuki, M.; Tagami, J. Evaluation of new treatment for incipient enamel demineralization using 45S5 bioglass. *Dent. Mater.* **2014**, *30*, 314–320. [[CrossRef](#)] [[PubMed](#)]
28. Johnsson, S.-A.; Nancollas, G.H. The role of brushite and octacalcium phosphate in apatite formation. *Crit. Rev. Oral. Biol. Med.* **1992**, *3*, 61–82. [[CrossRef](#)]
29. Rabizadeh, T.; Peacock, C.L.; Benning, L.G. Carboxylic acids: Effective inhibitors for calcium sulfate precipitation? *Mineral. Mag.* **2014**, *78*, 1465–1472. [[CrossRef](#)]
30. Wang, M.; Li, H.; Huang, X.; Yi, L. Zinc maleate and calcium stearate as a complex thermal stabilizer for Poly(Vinyl Chloride). *J. Vinyl Addit. Technol.* **2014**, *20*, 1–9. [[CrossRef](#)]
31. Bensalah, N.; Louhichi, B.; Abdel-Wahab, A. Electrochemical oxidation of succinic acid in aqueous solutions using boron doped diamond anodes. *Int. J. Environ. Sci. Technol.* **2012**, *9*, 135–143. [[CrossRef](#)]
32. Griesbach, U.; Malkowsky, I.M.; Waldvogel, S.R. Green electroorganic synthesis using BDD electrodes. In *Electrochemistry for the Environment*, 1st ed.; Comninellis, C., Chen, G., Eds.; Springer: New York, NY, USA, 2010; pp. 125–141.
33. McBeath, S.T.; Wilkinson, D.P.; Graham, N.J.D. Application of boron-doped diamond electrodes for the anodic oxidation of pesticide micropollutants in a water treatment process: A critical review. *Environ. Sci. Water Res. Technol.* **2019**, *5*, 2090–2107. [[CrossRef](#)]
34. Nidheesh, P.V.; Divyapriya, G.; Oturan, N.; Trellu, C.; Oturan, M.A. Environmental applications of boron-doped diamond electrodes: 1. Applications in water and wastewater treatment. *ChemElectroChem* **2019**, *6*, 2124–2142. [[CrossRef](#)]
35. Dirany, A.; Sirés, I.; Oturan, N.; Özcan, A.; Oturan, M.A. Electrochemical treatment of the antibiotic sulfachloropyridazine: Kinetics, reaction pathways, and toxicity evolution. *Environ. Sci. Technol.* **2012**, *46*, 4074–4082. [[CrossRef](#)]
36. Fu, B.; Yuan, J.; Qian, W.; Shen, Q.; Sun, X.; Hannig, M. Evidence of chemisorption of maleic acid to enamel and hydroxyapatite. *Eur. J. Oral Sci.* **2004**, *112*, 362–367. [[CrossRef](#)]
37. Göltz, M.; Koch, M.; Detsch, R.; Karl, M.; Burkovski, A.; Rosiwal, S. Influence of *in-situ* electrochemical oxidation on implant surface and Colonizing Microorganisms Evaluated by Scanning Electron Microscopy. *Materials* **2019**, *12*, 3977. [[CrossRef](#)]
38. Koch, M.; Göltz, M.; Xiangjun, M.; Karl, M.; Rosiwal, S.; Burkovski, A. Electrochemical disinfection of dental implants experimentally contaminated with microorganisms as a model for periimplantitis. *J. Clin. Med.* **2020**, *9*, 475. [[CrossRef](#)] [[PubMed](#)]
39. Cuscó, R.; Guitián, F.; de Aza, A.; Artús, L. Differentiation between hydroxyapatite and β -tricalcium phosphate by means of μ -raman spectroscopy. *J. Eur. Ceram. Soc.* **1998**, *18*, 1301–1305. [[CrossRef](#)]
40. Miller, M.A.; Kendall, M.R.; Jain, M.K.; Larson, P.R.; Madden, A.S.; Tas, A.C. Testing of brushite ($\text{CaHPO}_4 \cdot 2 \text{H}_2\text{O}$) in synthetic biomineralization solutions and in situ crystallization of brushite micro-granules. *J. Am. Ceram. Soc.* **2012**, *95*, 2178–2188. [[CrossRef](#)]
41. Boanini, E.; Silingardi, F.; Gazzano, M.; Bigi, A. Synthesis and hydrolysis of brushite (DCPD): The role of ionic substitution. *Cryst. Growth Des.* **2021**, *21*, 1689–1697. [[CrossRef](#)]
42. Kalantar Motamedi, M.R.; Mortaheb, A.; Zare Jahromi, M.; Gilbert, B.E. Micro-CT evaluation of four root canal obturation techniques. *Scanning* **2021**, *2021*, 6632822. [[CrossRef](#)] [[PubMed](#)]
43. Zuolo, M.L.; Zaia, A.A.; Belladonna, F.G.; Silva, E.J.N.L.; Souza, E.M.; Versiani, M.A.; Lopes, R.T.; De-Deus, G. Micro-CT assessment of the shaping ability of four root canal instrumentation systems in oval-shaped canals. *Int. Endod. J.* **2018**, *51*, 564–571. [[CrossRef](#)] [[PubMed](#)]

44. Bannerman, A.; Williams, R.L.; Cox, S.C.; Grover, L.M. Visualising phase change in a brushite-based calcium phosphate ceramic. *Sci. Rep.* **2016**, *6*, 32671. [[CrossRef](#)] [[PubMed](#)]
45. Lafuente, B.; Downs, R.T.; Yang, H.; Stone, N. The power of databases: The RRUFF project. In *Highlights in Mineralogical Crystallography*, 1st ed.; Armbruster, T., Danisi, R.M., Eds.; De Gruyter: Berlin, Germany; Munich, Germany; Boston, MA, USA, 2015; pp. 1–30.
46. Montes-Hernandez, G. Nucleation of brushite and hydroxyapatite from amorphous calcium phosphate phases revealed by dynamic in situ raman spectroscopy. *J. Phys. Chem. C* **2020**, *124*, 15302–15311. [[CrossRef](#)]
47. Penel, G.; Leroy, N.; van Landuyt, P.; Flautre, B.; Hardouin, P.; Lemaître, J.; Leroy, G. Raman microspectrometry studies of brushite cement: In vivo evolution in a sheep model. *Bone* **1999**, *25*, 81–84. [[CrossRef](#)]